



Brainstem atrophy in the early stage of Alzheimer's disease: a voxel-based morphometry study

Xiaoxi Ji^{1,2,3} · Hui Wang³ · Minwei Zhu⁴ · Yingjie He^{2,3} · Hong Zhang^{2,3} · Xiaoguang Chen³ · Wenpeng Gao¹  · Yili Fu¹ · for the Alzheimer's Disease Neuroimaging Initiative

Published online: 2 January 2020

© Springer Science+Business Media, LLC, part of Springer Nature 2020

Abstract

Postmortem studies on patients with Alzheimer's disease (AD) have confirmed that the dorsal raphe nucleus (DRN) in the brainstem is the first brain structure affected in the earliest stage of AD. The present study examined the brainstem in the early stage of AD using magnetic resonance (MR) imaging. T1-weighted MR images of the brains of 81 subjects were obtained from the publicly available Open Access Series of Imaging Studies (OASIS) database, including 27 normal control (NC) subjects, 27 patients with very mild AD (AD-VM) and 27 patients with mild AD (AD-M). The brainstem was interactively segmented from the MR images using ITK-SNAP. The present voxel-based morphometry (VBM) study was designed to investigate the brainstem differences between the AD-VM/AD-M groups and the NC group. The results showed bilateral loss in the pons and the left part of the midbrain in the AD-M group compared to the NC group. The AD-M group showed greater loss in the left midbrain than the AD-VM group ($P_{FWEcorrected} < 0.05$). The results revealed that brainstem atrophy occurs in the early stages of AD (Clinical Dementia Rating = 0.5 and 1.0). Most of these findings were also investigated in a multicenter dataset. This is the first VBM study that provides evidence of brainstem alterations in the early stage of AD.

Keywords Brainstem · Magnetic resonance imaging · Voxel-based morphometry · Alzheimer's disease

Introduction

Alzheimer's disease (AD) is the most common form of dementia in people older than 65 years. AD is a chronic neurodegenerative disease that progressively impairs memory and cognitive function, and interferes with daily life. According to

neuropathological findings, AD is characterized by the accumulation of extracellular amyloid- β ($A\beta$), which results in senile plaques (SPs) and intracellular phosphorylated tau protein that forms neurofibrillary tangles (NFTs). These characteristics result in neuronal and synaptic loss, a decrease in cerebral cortex cells and the occurrence of amyloidosis in cortical arteries (Hellström-Lindahl et al. 2009). These changes can affect people's memory, cognition, activity, and sleep-wake cycle.

Major efforts have been made to find a biological marker that would enable the early detection of AD and thus allow early interventions. However, measuring these biochemical markers requires collecting a CSF sample, which is invasive and not always acceptable to AD patients. Mental status and mood testing are always given before standard medical tests. These tests cannot rule out other possible causes of symptoms. Recently, the use of magnetic resonance imaging (MRI) to aid in the diagnosis of AD has attracted a great deal of research interest in recent years, because MRI is noninvasive and free of ionizing radiation. Many MRI studies have assessed differences in brain areas between AD patients and healthy controls. The most consistent finding is the atrophy in medial temporal

Xiaoxi Ji, Hui Wang and Minwei Zhu contributed equally to this work.

✉ Xiaoguang Chen
xgchen0415@outlook.com

✉ Wenpeng Gao
wpgao@hit.edu.cn

¹ School of Life Science and Technology, Harbin Institute of Technology, Building 2E-417, 2 Yikuang Street, Nangang District, Harbin, Heilongjiang Province, China

² Guangzhou Medical University, Guangzhou, China

³ Department of Neurosurgery, Third People's Hospital of Hainan Province, 146 Jiefang Road, Sanya, Hainan Province, China

⁴ Department of Neurosurgery, First Affiliated Hospital of Harbin Medical University, Harbin, China

lobe structures including the hippocampus, amygdala, transentorhinal/entorhinal cortex and parahippocampal gyrus (Karas et al. 2007; Samuraki et al. 2007; Kinkingnéhun et al. 2008; Schuff et al. 2009), which is consistent with the pathological changes that occur in early AD. As the disease progresses, other brain regions, such as the thalamus, temporal lobe, corpus callosum (Zhu et al. 2012, 2014), cingulate and frontal lobe, also lose volume. Longitudinal studies using MRI measurements have demonstrated that the pattern of atrophy correlates well with the progression of NFTs observed in pathology. There have been many studies of AD related brain structural changes in vivo. In 2009, a postmortem brain study revealed that the dorsal raphe nucleus (DRN) showed an accumulation of NFTs before the Braak staging system's transentorhinal region (Grinberg et al. 2009). This finding suggested that the brainstem was affected by AD before the supratentorial regions. The brainstem is recognized as the central axis of the brain, with many nuclei that regulate various functions, such as respiratory function, heart rhythm, and cognition. The goal of this study is to examine brainstem alterations in relation to AD.

Analysis tools, such as voxel-based morphometry (VBM)¹ and FreeSurfer², are very important in detecting changes of brain structures in AD. FreeSurfer is a suite of tools used to analyze brain images, to quantify the functional and structural properties of the human brain and to determine brain connectivity (Fischl 2012). The software provides the dominant surface-based method used to assess the local concentration of gray matter (GM) and/or white matter (WM) in the same stereotactic space (Ashburner and Friston 2000; Walhovd et al. 2005; Tae et al. 2008; Celle et al. 2016). FreeSurfer has been widely used in neuroimaging analyses of neuropsychological diseases, such as AD, Parkinson's disease, and multiple sclerosis. Relative to FreeSurfer, VBM is more sensitive to the location of changes. In particular, VBM may help determine the best biological markers to aid in the diagnosis of incipient AD and to identify individuals with an increased risk of developing dementia. To the best of our knowledge, this is the first study to investigate brainstem changes in patients with early AD using VBM.

In this study, we investigated the differences in the brainstem between individuals with AD and healthy elderly individuals using VBM. MRI volumes of 162 subjects were selected from two publicly available datasets. The brainstem was delineated in each MRI volume using ITK-SNAP.³ A dedicated protocol for the morphometric analysis of the segmented brainstem was used to locate the brainstem changes in the early stage of AD using VBM.

¹ <https://www.fil.ion.ucl.ac.uk/spm/>

² <https://surfer.nmr.mgh.harvard.edu/>

³ www.itksnap.org

Materials and methods

Data acquisition

Data used in this study were obtained from the Open Access Series of Imaging Studies (OASIS) cross-sectional database⁴ (Zhang et al. 2001; Buckner et al. 2004; Fotenos et al. 2005; Marcus et al. 2007), which was made freely available by Dr. Randy Buckner at Harvard University, the Neuroinformatics Research Group at Washington University and the Biomedical Informatics Research Network. The database contains three-dimensional (3D) sagittal T1-weighted magnetization-prepared rapid gradient-echo (MP-RAGE) structural MRI brain scans acquired on a 1.5-T Vision scanner (Siemens, Erlangen, Germany) from 416 right-handed subjects ranging in age from 18 to 96 years. The MP-RAGE parameters were empirically optimized for gray–white contrast (Table 1). In OASIS, AD subjects' dementia status was quantified in terms of Clinical Dementia Rating (CDR) scale (Morris 1993; Rubin et al. 1998). A global CDR of 0 indicates no dementia, and CDRs of 0.5, 1, 2, and 3 represent very mild, mild, moderate, and severe dementia, respectively. Details on subject age and sex distribution, demographics, inclusion/exclusion criteria, and preprocessing steps have been provided in the literature (Marcus et al. 2007). In this study, 81 subjects between 65 and 90 years of age with a CDR range of 0 to 1 were selected and subdivided into three groups, namely, the normal control (NC) group (CDR = 0), the very mild AD (AD-VM) group (CDR = 0.5) and the mild AD (AD-M) group (CDR = 1). Each AD subject was matched by age- and sex to an NC subject. Further details about each group are summarized in Table 2.

To enhance the statistical power and the generalizability of the findings, we also selected 81 subjects from the Alzheimer's Disease Neuroimaging Initiative (ADNI) database⁵ with the same inclusion criteria mentioned above. Details on these subjects are also shown in Table 2. In addition, the ADNI provides Neuropsychiatric Inventory Questionnaire (NPI-Q) scores measuring the presence and severity of neuropsychiatric symptoms (NPS) in patients with dementia.

VBM was originally designed for automated quantitative analysis of the distribution of GM and WM rather than the brainstem. A dedicated protocol of VBM-based analysis of the brainstem is proposed in Fig. 1.

Brainstem segmentation using ITK-SNAP

The brainstem consists of the midbrain, pons and medulla oblongata. It is difficult to distinguish the brainstem from

⁴ <http://www.oasis-brains.org>

⁵ <http://adni.loni.usc.edu>

Table 1 Details of MRI Acquisition

	OASIS	ADNI
Vendor	Siemens	Siemens/GE/Philips
Sequence	MP-RAGE	MP-RAGE
TR(msec)	9.7	2300~2400
TE(msec)	4.0	3.5
Flip angle(°)	10	8
TI(msec)	20	1000
TD(msec)	200	–
Orientation	Sagittal	Sagittal
Thickness, gap(mm)	1.25, 0	1.2, 0
Field of View	256 × 256	240 × 240
Voxel size(mm ³)	1 × 1 × 1	0.94 × 0.94 × 1.2

adjacent non-brainstem structures (cerebellar peduncles and cerebrum) due to similar signal intensity in structural MRI. The criteria used to discriminate the brainstem from the neighboring structures are shown in Fig. 2. The superior boundary between the brainstem and cerebrum is on the axial slice where the optic tract appears. The inferior boundary is at the level of the foramen magnum. The lateral boundary begins in the sagittal plane where the lateral geniculate body and optic nerve appear. The posterior boundary begins when an anterior protrusion appears from the cerebellum in the sagittal view, and contains the lateral part of the bulbopontine sulcus, which forms the junction of the medulla, the pons and the cerebellum and sends out the vestibulocochlear nerve. In addition, the cranial nerves, arteries and veins around the brainstem were excluded from the outline when discernible.

Brainstem segmentation was achieved using ITK-SNAP, which provides semiautomatic segmentation using the active contour method as well as manual delineation (Paul et al. 2006). First, semiautomatic segmentation was used to coarsely extract the brainstem from MR volumes in four steps: (1) specifying the region of interest (ROI) of the brainstem; (2) adjusting the dual-threshold to coarsely isolate the brainstem from surrounding structures in the ROI; (3) placing several bubbles with a certain radius (set at 3 mm) inside the segmented brainstem; and (4) expanding the bubbles to fill the entire brainstem. Then, manual delineation was performed to correct the coarsely segmented brainstem according to the criteria described above.

In order to determine the inter-rater reliability of the segmentation method, 10 subjects were randomly selected from each group, i.e., a total of 30 subjects. Two raters blind to the subjects' CDR classification were asked to segment the brainstem using ITK-SNAP following the protocol described above. The volume of the brainstem as segmented by each of the two raters was calculated as the voxel count multiplied by the voxel size. The degree of agreement between the two raters was assessed in terms of correlation. The volumes

Table 2 Demographic and clinical characteristics of all participants

	OASIS				ADNI				<i>p</i> value
	NC group	AD-VM group	AD-M group	<i>p</i> value	NC group	AD-VM group	AD-M group	<i>p</i> value	
CDR	0	0.5	1.0	–	0	0.5	1.0	–	–
Number	27	27	27	–	27	27	27	–	–
Sex (male/female)	6/21	11/16	9/18	$\chi^2 = 2.126, p = 0.345$	13/14	17/10	13/14	$\chi^2 = 1.586, p = 0.452$	$F = 0.438, p = 0.647$
Age [(mean ± SD (years))]	77.00 ± 7.27	75.26 ± 6.22	77.07 ± 6.12	$F = 0.663, p = 0.518$	76.41 ± 4.94	74.89 ± 8.19	75.07 ± 5.99	–	–
Educational level* [(mean ± SD)]	3.15 ± 1.49	2.93 ± 1.20	2.48 ± 1.25	$F = 1.784, p = 0.175$	–	–	–	–	–
NPI-Q (mean ± SD)	–	–	–	–	–	2.74 ± 2.19	6.48 ± 4.06	$t = -4.211, p = 0.000$	–
MMSE (mean ± SD)	28.89 ± 1.34	25.67 ± 3.51	21.52 ± 3.73	$F = 51.483, p = 0.000$	28.96 ± 1.16	23.85 ± 3.23	20.19 ± 3.71	$F = 61.604, p = 0.000$	–
BSV [(mean ± SD(mm ³))]	30.881 ± 3682	28.627 ± 2963	27.109 ± 2655	$F = 9.93, p = 0.000$	26.309 ± 2679	27.342 ± 2357	24.965 ± 2935	$F = 5.328, p = 0.000$	–
nBSV [(mean ± SD)]	0.022 ± 0.004	0.019 ± 0.003	0.018 ± 0.002	$F = 6.439, p = 0.003$	0.0166 ± 0.0015	0.0173 ± 0.0014	0.0161 ± 0.0015	$F = 4.176, p = 0.02$	–

* Educational level: 1-less than high school grad, 2-high school grad, 3-some college, 4-college grad, 5-beyond college

- Not available

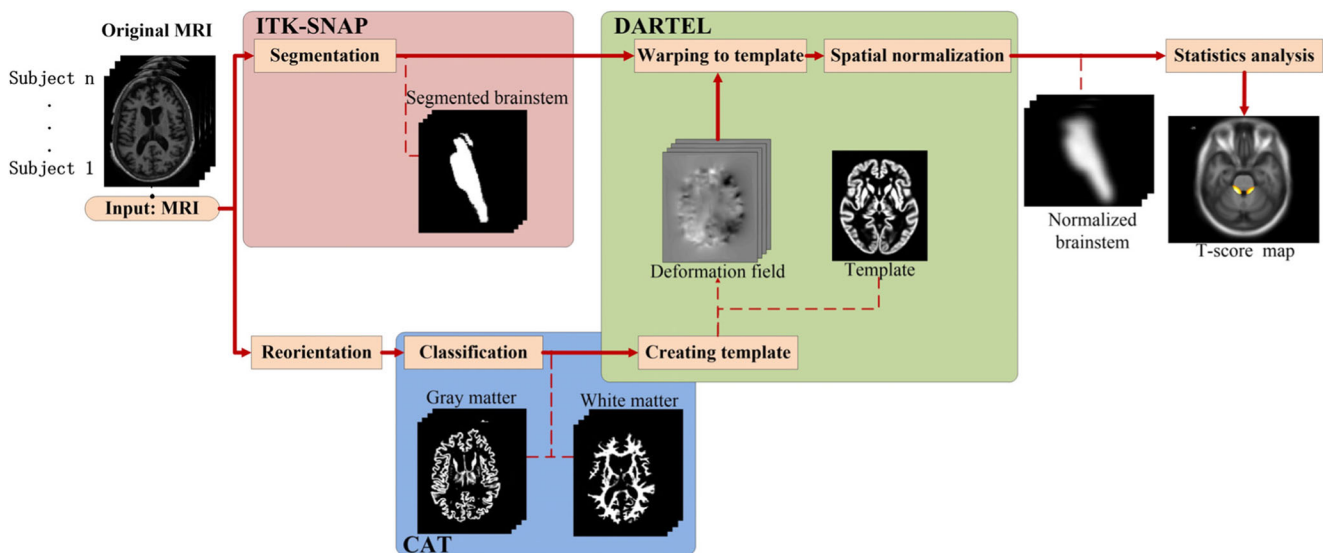


Fig. 1 The protocol for VBM-based analysis of the brainstem. First, the brainstem is segmented using ITK-SNAP (Yushkevich et al., 2006). Subsequent image processing and analysis was performed with SPM12 (Wellcome Trust Centre for Neuroimaging, London, UK) running on MATLAB R2016b (The MathWorks, Inc., Sherborn, MA, USA) (Ashburner and Friston 2000). All MR volumes are classified into GM and WM using the Computational Anatomy Toolbox (CAT). With the

GM and WM, a customized template is created using the Diffeomorphic Anatomical Registration Through Exponential Lie Algebra (DARTEL), and deformation fields are generated. Each segmented brainstem is warped to the template with the corresponding deformation field followed by spatial normalization to the MNI space. The normalized brainstems in different groups then undergo voxel-wise statistical analysis

obtained by two raters were positively correlated ($r = 0.937$, $p = 0.000$). The overlap of the segmented brainstem by two raters was measured by the Dice similarity coefficient (DSC). The mean \pm standard deviation DSC was 0.92 ± 0.01 . We also compared our segmentation results with those generated by FreeSurfer and found that the mean \pm standard deviation DSC was 0.90 ± 0.02 . Figure 3 illustrates the brainstem segmentation results with ITK-SNAP and FreeSurfer. Our method takes approximately 20 min to segment a brainstem from an MR volume. This method saves a considerable amount of time compared to FreeSurfer (which takes approximately 10 hours for preprocessing of one subject plus 8 min for brainstem labeling).

Image processing using statistical parametric mapping (SPM)

For VBM analysis, all segmented brainstems are typically normalized into a standard space, but this is difficult to achieve with only the segmented brainstem images owing to the lack of spatial information of the whole brain. Whole-brain MR volumes were used to assist in the spatial normalization of the segmented brainstem using SPM12. The procedure consisted of the following five steps (shown in Fig. 1).

- (1) **Reorientation.** Each MR volume in the OASIS dataset had already been reoriented to make the anterior

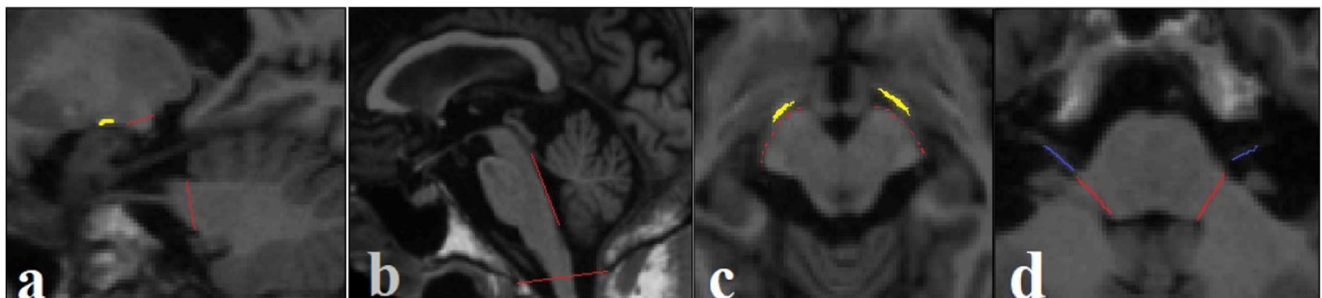


Fig. 2 Boundaries (red) of the brainstem defined in different views. (a) The lateral boundary in the sagittal view on which the lateral geniculate body and the optic nerve (yellow) appears. The posterior boundary begins when anterior protrusion appears from the cerebellum in the sagittal view. (b) The inferior boundary at the level of foramen magnum. The lateral boundary in the sagittal view on which the lateral geniculate body

and the optic nerve (yellow) appears. The posterior boundary begins when anterior protrusion appears from the cerebellum in the sagittal view. (c) The superior boundary in the axial view in which the optic nerve of diencephalon appears. (d) The posterior boundary also contains the lateral part of the bulbopontine sulcus sending out the vestibulocochlear nerve (blue)

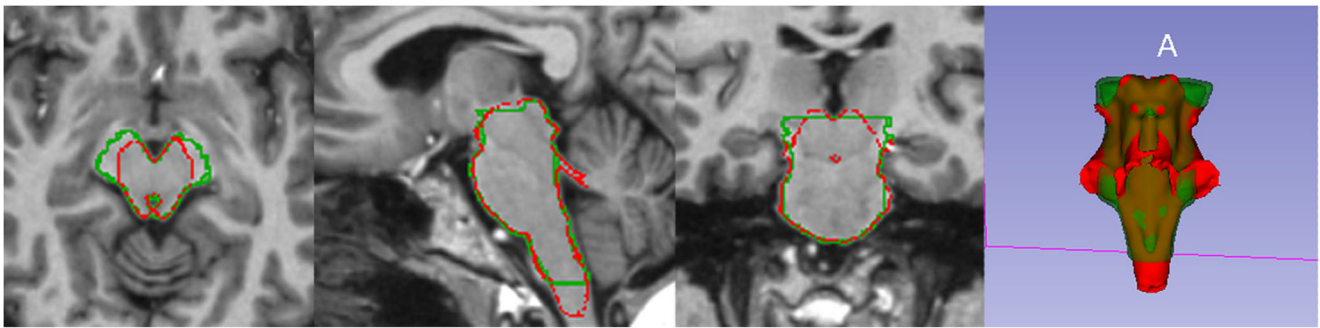


Fig. 3 Segmented brainstem contours using ITK-SNAP (green) and FreeSurfer (red) overlaid on the MR image. From left to right, axial view, sagittal view, coronal view and surface rendering

commissure-posterior commissure (AC-PC) line horizontal. The AC was localized on the midsagittal plane of each MR volume was localized.

- (2) **Classification.** The Bayesian probability of each voxel for each tissue type (i.e., GM and WM) was calculated using the Computational Anatomy Toolbox (CAT) with a tissue probability map. The International Consortium of Brain Mapping (ICBM) template was used as prior knowledge.
- (3) **Creating a template.** A customized template was created by iteratively aligning all MR volumes using the diffeomorphic anatomical registration through exponential lie algebra (DARTEL) toolbox, which is a high-dimensional warping process to increase registration accuracy. DARTEL works by aligning GM and WM among the images, which is achieved by modeling the shape of each brain. A deformation field from each subject to the template is generated when the template is created.
- (4) **Warping to the template.** Each segmented brainstem using ITK-SNAP was warped to the template using the corresponding deformation field. This measure reduced the inter-subject variability.
- (5) **Spatial normalization.** Spatial normalization was used to fit each individual brain to the tissue probability maps (TPMs) provided by SPM to accommodate different brain sizes and shapes. The warped brainstem images were modulated using Jacobian determinants to preserve regional volumetric information, and smoothed with an 8-mm full-width at half-maximum (FWHM) isotropic Gaussian kernel to increase the signal-to-noise ratio.

Statistical analysis

The brainstem volume (BSV) of each subject was measured by multiplying the voxel size by the number of voxels in the segmented brainstem region. The normalized brainstem volume (nBSV) was then calculated as the result of the division

of BSV by the estimated total intracranial volume (eTIV) to account for inter-subject variability in brain size.

Demographics, education levels, and Mini-Mental State Examination (MMSE) scores were analyzed using SPSS 22.0 (IBM Corp., Somers, NY, USA). Prior to the analysis, the Shapiro-Wilk test was used to determine whether the data were distributed normally. Analysis of variance (ANOVA) was used to determine if there was a significant difference among the three groups in terms of age, educational level, MMSE score, or brainstem volume. The associations of nBSV (the ratio of the measured brainstem volume to the estimated total intracranial volume) with MMSE scores and age were assessed by Pearson's correlation analysis. Differences in sex distribution were determined using a chi-square test. Significant results are reported at a voxel-level p value <0.05 . A nonparametric method was used due to skewness in the numeric clinical variables.

Volume measurements can be used to determine the differences in total brainstem volume, but do not provide information about where these differences occur. VBM-based analysis of the brainstem (as described above) was performed to compare the three groups and locate where the differences occurred. The normalized, modulated, smoothed brainstem images of three groups were compared by employing the general linear model framework in SPM12. In the factorial design, we set an absolute threshold (threshold = 0.1) to mask the brainstem so that only voxels with a value exceeding the threshold were included in the analysis. An ANOVA model was computed to assess the differences in brainstem volume among the three groups. The estimated total intracranial volume (eTIV), age, sex, education level and MMSE scores were included in the model as nuisance variables. The difference in brainstem volume between each pair of groups was assessed using a two-sample t -test. For all SPM analyses, a significance level of $P < 0.05$, chosen a priori, was considered statistically significant with family-wise error (FWE) correction applied for multiple comparisons at a cluster level (Ridgway et al. 2008).

Results

Demographic data analysis

The OASIS data recording the total brainstem volume in each group are summarized in Table 2. There was no significant difference ($\chi^2 = 2.126$, $p = 0.345$) in male/female distributions among the three groups. There was no significant age difference ($F = 0.663$, $p = 0.518$) among the three groups. As expected, nBSV was significantly different ($F = 6.439$, $p < 0.005$) among the three groups. The mean brainstem volume of the AD-M group ($27,109 \text{ mm}^3$) was smaller than that of the NC group ($30,881 \text{ mm}^3$) or the AD-VM group ($28,627 \text{ mm}^3$). There was no correlation between nBSV and MMSE scores ($\gamma = 0.187$, $p = 0.094$). Additionally, no correlation between nBSV and age was found in the NC group ($\gamma = 0.02$, $p = 0.923$).

The demographic and clinical characteristics of the ADNI data are summarized in Table 2. There was no significant difference ($\chi^2 = 1.586$, $p = 0.452$) in male/female distributions among the three groups. There was no significant age difference ($F = 0.438$, $p = 0.647$) among the three groups. Similarly, the nBSV was significantly different ($F = 4.176$, $p < 0.05$) among the three groups. However, the mean brainstem volume of the AD-VM group ($27,342 \text{ mm}^3$) was larger than that of the NC group ($26,309 \text{ mm}^3$) or the AD-M group ($24,965 \text{ mm}^3$). There was no correlation between nBSV and MMSE scores ($\gamma = 0.039$, $p = 0.728$). No correlation between nBSV and age was found in the NC group ($\gamma = -0.111$, $p = 0.325$). The comparison of the samples according to the severity of dementia (CDR = 0.5 and CDR = 1) revealed an increase in NPI-Q scores as the disease progressed. However, there was no correlation between nBSV and NPI-Q ($\gamma = -0.213$, $p = 0.123$).

VBM analysis

The volume measurements described above are useful for determining differences between groups in the brainstem as a whole but do not reveal exactly where these differences occur. VBM-based analysis of the brainstem in the three groups was

performed to locate the differences following the described protocol. The ANOVA results of the OASIS data show that there were significant differences in two areas of the brainstem among the three groups ($F = 9.361$, $p < 0.05$). These differences were found in the pons and midbrain (Table 3). No significant differences were found in the medulla oblongata. We individually compared each group to the other two groups using a two-sample *t*-test and found that brainstem atrophy occurs at different locations in different stages of AD. Figures 4 and 5 illustrate the significant atrophic areas overlaid onto the ICBM 152 template. Compared with the NC group, the AD-VM group had no significant difference in brainstem, while the AD-M group showed large-scale reductions in the pons and midbrain (Fig. 5, Table 4; $P_{FWEcorrected} < 0.05$). Table 5 summarizes the significant differences between the AD-VM group and the AD-M group in terms of the brainstem volume in the left part of the midbrain. Overall, the left part of the midbrain was the first brainstem area to atrophy in the AD-VM group (CDR = 0.5).

In addition, we combined the two datasets together, referred to as OASIS+ADNI, and performed the analysis following the protocol mentioned above. The ANOVA results showed that there were significant differences in two areas of the brainstem (midbrain and pons) among the three groups (Table 3). The atrophy of the left brainstem was more severe than that of the right brainstem. Compared with the NC group, the AD-VM group showed no significant differences in the brainstem, whereas the AD-M group showed volume reductions in the pons and midbrain (Table 4, $P_{FWEcorrected} < 0.05$). However, we did not find a volume decrease in the pons and midbrain between the AD-VM group and the AD-M group (Table 5). Figures 4 and 5 show the significance maps of brainstem volume from the ANOVA and two-sample *t*-tests.

Discussion

The present study used a VBM-based analysis to detect the brainstem differences between AD patients and NC. VBM could also be used to examine other brain structures affected by AD.

Table 3 Brainstem volume differences between the three groups (NC, AD-VM and AD-M)

Region	OASIS			<i>F</i>	OASIS+ADNI			<i>F</i>		
	Cluster size	MNI coordinates (mm)			Cluster size	MNI coordinates (mm)				
		x	y			z	x		y	z
Right pons	48	13	-35	-30	13.26	23	12	-36	-30	12.4
Left pons	247	-10	-32	-27	10.6	209	-9	-36	-29	11.84
Left midbrain	242	-13	-26	-3	11.69	64	-6	-36	-24	9.75

NC normal controls (CDR = 0), AD-VM very mild AD patients (CDR = 0.5), AD-M mild AD patients (CDR = 1.0)

Results are reported at $P_{FWEcorrected} < 0.05$

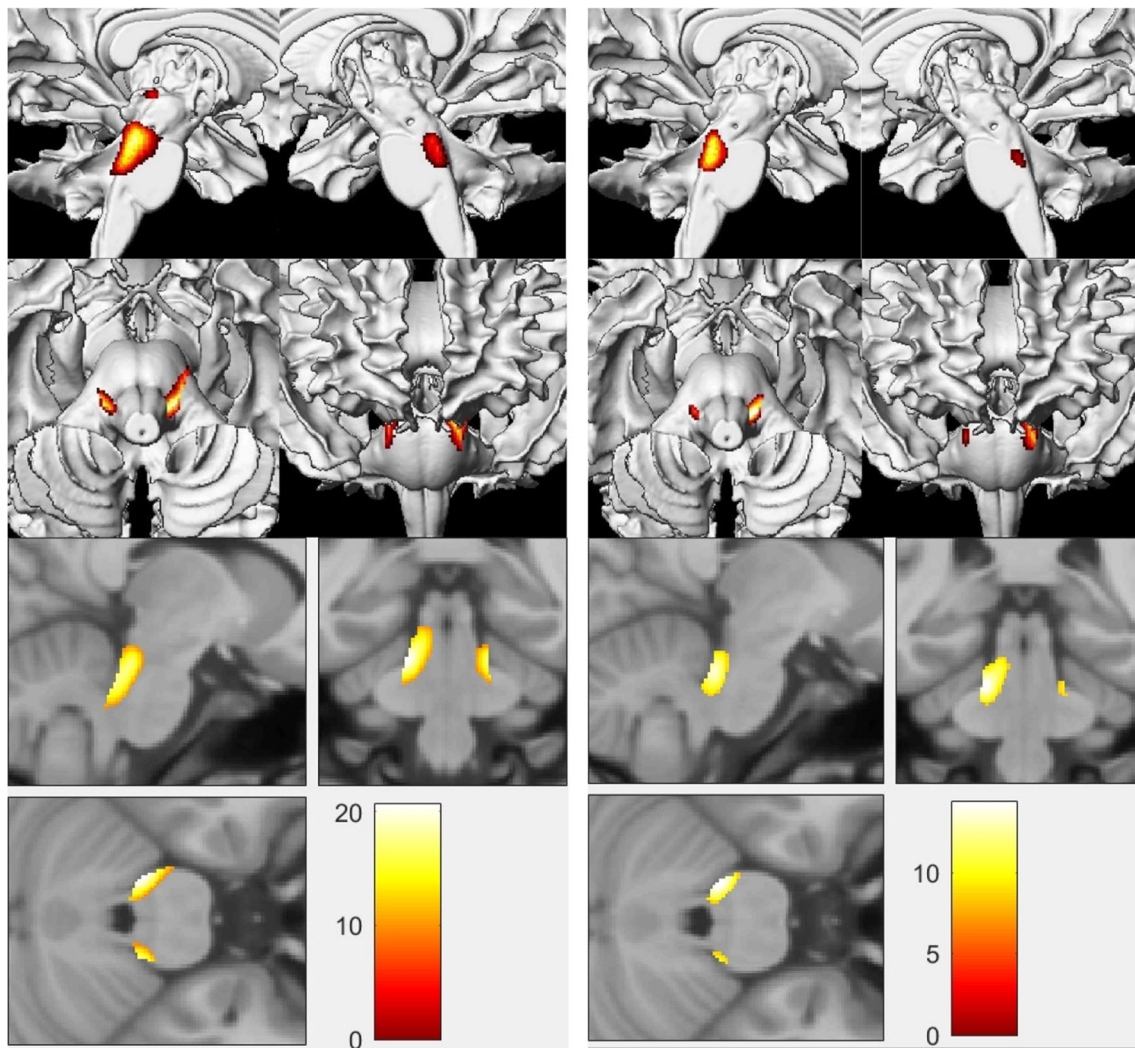


Fig. 4 Anova analysis between the three groups ($P_{FWEcorrected} < 0.05$) in OASIS (left) and OASIS+ADNI (right)

The structural changes found in this study may be one site of early pathological changes in AD. To the best of our knowledge, this is the first VBM-based study of AD patients' brainstems.

To date, few studies have examined brainstem changes in AD patients using MRI. Mrzilková et al. (2012) used manual volumetric measurement to compare the brainstems of 26 AD patients with the brainstems of 29 normal controls and concluded that unlike the volume decreases observed in the hippocampus, there was no volume decrease in the pons nor was there significant left-right asymmetry in pons. In contrast, Lee and colleagues (Lee et al. 2015) used FreeSurfer to analyze the volume and shape of AD patients' brainstems and found that the total volume of the brainstem in AD patients was significantly reduced and that deformation occurred in the upper posterior brainstem corresponding to the midbrain. No left-right asymmetry in the brainstem was reported. There are several reasons for these inconsistent or even contradictory findings. First, different segmentation methods were used based on different boundary definitions (see Fig. 3). The

manual segmentation method used by Mrzilková and colleagues is the most common method, but it has many drawbacks. It is subjective, error prone and labor intensive. Automatic segmentation methods such as FreeSurfer are more objective. However, FreeSurfer cannot completely segment the brainstem and misses some important structures, such as the substantia nigra in the midbrain (Hwang et al. 2011; Weier et al. 2012; Wang et al. 2016). In our study, segmentation of the entire brainstem was achieved using the active contour method followed by manual correction. This method showed efficiency (approximately 20 min per subject) and high inter-rater reliability (DSC: 0.92 ± 0.01 ; correlation: $r = 0.937$, $p = 0.000$). Second, different analysis methods were used. Geometric measurements (such as the area or volume of the structure) can reveal a change in the whole structure without revealing the location of the change. FreeSurfer can accurately determine cortical thickness but cannot pinpoint the location of certain morphological changes. VBM-based methods can determine the anatomical differences at the voxel level and

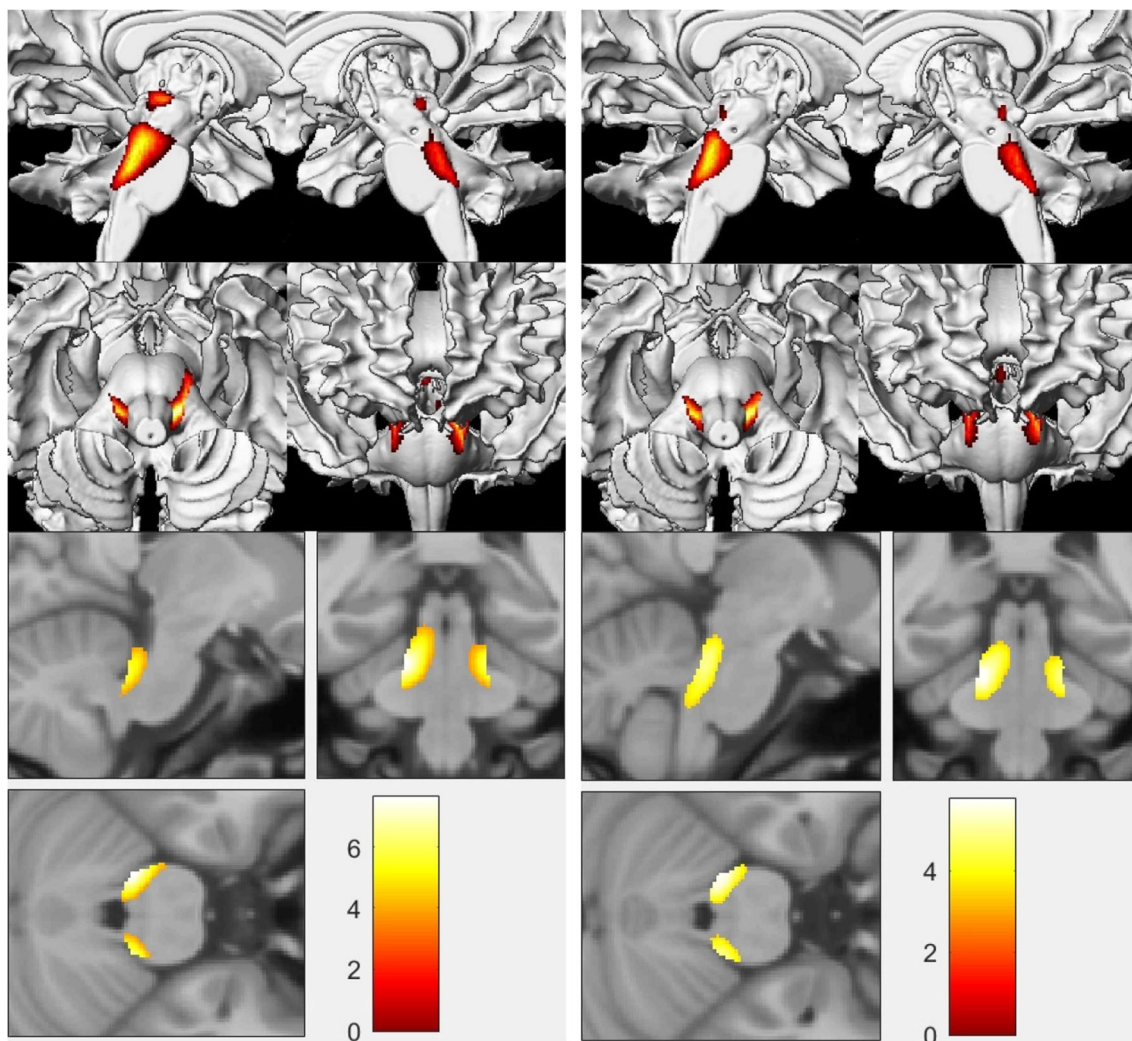


Fig. 5 Significance maps of AD-M group compared with NC group ($P_{FWEcorrected} < 0.05$) in OASIS (left) and OASIS+ADNI (right)

evaluate small changes in morphology (Wright et al. 1995; Ashburner and Friston 2000; Busatto et al. 2008). Last, different studies enrolled different types of subjects. Lee's and Mrzilková's studies mostly focused on mild and moderate AD patients ($CDR = 1$ and 2) and do not include the early AD cases ($CDR = 0.5$). Our study included a set of very mild

AD patients ($CDR = 0.5$) to investigate whether brainstem atrophy occurred in the earliest stage of AD.

We compared the OASIS brainstem data in different stages of AD with those of NC following the previously described protocol. The volumes of the bilateral pons and midbrain were significantly decreased in the AD-VM and AD-M groups (Figs. 4

Table 4 Two-sample *t*-Test comparing the AD-M group and the NC group

Region	OASIS				<i>t</i>	OASIS+ADNI				<i>t</i>
	Cluster size	MNI coordinates (mm)				Cluster size	MNI coordinates (mm)			
		x	y	z			x	y	z	
Right pons	148	13	-35	-31	4.95	319	11	-36	-29	4.62
Left pons	514	-10	-35	-30	5.68	545	-9	-36	-30	4.97
Left midbrain	509	-6	-35	-18	4.69	192	-5	-36	-21	3.97

AD-M mild AD patients ($CDR = 1$), NC normal controls ($CDR = 0$). Results are reported at $P_{FWEcorrected} < 0.05$

Table 5 Two-sample *t*-Test comparing the AD-VM group and AD-M group from OASIS

OASIS					OASIS+ADNI					
Region	Cluster size	MNI coordinates (mm)			<i>t</i>	Cluster size	MNI coordinates (mm)			<i>t</i>
		x	y	z			x	y	z	
Left midbrain	5	-10	-31	-17	3.88	null	null	null	null	null

AD-VM very mild AD patients (CDR = 0.5), AD-M mild AD patients (CDR = 1). Results are reported at $P_{FWEcorrected} < 0.05$

null: no significant difference exist

and 5), which indicated that the brainstems of AD patients undergo atrophy. This finding is consistent with the neuronal pathology revealed by previous postmortem studies (Rüb et al. 2000; Grudzien et al. 2007; Grinberg et al. 2009; Grudzien et al. 2007; Grinberg et al. 2011; Attems et al. 2012; Rodríguez et al. 2012; Wilson et al. 2013). These studies found that there is cell loss or neuropathologic changes (tau lesions and deposition of A β protein) in AD patients' brainstems, particularly in the pons and midbrain. Compared with the NC group, no significant difference was found in the AD-VM group. The volume decrease was found in the left part of the midbrain in the AD-M group in comparison with the AD-VM group. No significant atrophy was investigated in the right part of the midbrain between these two consecutive stages. However, in comparison with the NC group, the volume of bilateral pons and the left part of the midbrain showed a significant decrease in the AD-M group. This phenomenon further consolidates the theory that AD is a progressive neurodegenerative disease. In the progression from normal to mild AD, the neurons in the pons and the left part of the midbrain degenerate, and this cumulative effect finally presents as significant atrophy in the pons and left part of the midbrain in the AD-M group in comparison with the NC group.

The atrophy that occurs in the left part of brainstem is more severe than the right counterpart in both the AD-VM and AD-M groups (Figs. 4 and 5). The left part of the midbrain first exhibits atrophy in the AD-VM group (CDR = 0.5). As the disease progresses, the right part also begins to atrophy as observed in the AD-M group (CDR = 1). Whether this phenomenon is related to right-handedness is unknown because no left-handed subjects were included in OASIS. However, asymmetric atrophy has also been observed in the hippocampi of AD patients (Mungas et al. 2002; Chetelat and Baron 2003; Shi et al. 2009). These two phenomena may be related.

To eliminate the factor of age, we examined the relationship between nBSV reductions and increases in age in the NC group. No correlation between nBSV and age (ranges 65–90 years) was observed in the NC group. In other words, aging has no effect on brainstem atrophy. This indicated that AD patients' nBSV decreases in relation to the progression of AD. There was no correlation between nBSV and MMSE scores.

In the OASIS+ADNI data study, the analysis also showed significant atrophy in the pons and midbrain in the AD patients

group compared with the NC group, especially in the left part. There were no significant differences between the NC group and the AD-VM group. We speculated that the progression from normal to very mild AD patients may be subtle and not yet morphologically manifested. These results were not exactly in agreement with those of the OASIS data study, probably because of MRI scans from different scanners running different acquisition protocols in a multicenter design (see Table 1).

The NPI-Q distress scale has been shown to be strongly and very significantly associated with the severity of NPS (Musa et al. 2017). In this study, we did not find correlation between the brainstem volume and the NPI-Q score. The negative correlation coefficient indicated the brainstem volume decreased as the NPS became severe.

The statistical power of imaging studies and the generalizability of the results will be increased by combining MRI scans from multiple centers to overcome single-site recruitment limitations (Takao et al. 2014). However, combining MRI scans from multiple centers can also introduce variance and systematic error negating these potential benefits, owing to the lack of a consistent acquisition protocol for the two datasets. Sources of scanner-related image variation include hardware differences (vendor, coil type, and field strength), acquisition parameters, etc. These factors may contribute to the difference in the findings in OASIS and OASIS+ADNI analyses (see Table 5). Nevertheless, the brainstem shows the trend of atrophy as AD progresses.

This study does not allow us to conclude the cause-effect relationship for AD; instead, it merely makes an attempt to identify structural changes in the brainstem. There are some limitations to this study. First, this is a cross-sectional study of the brainstem in the early stages of AD. Longitudinal studies are needed to verify the observed brainstem changes over the clinical course of AD. Second, only right-handed subjects were used because no left-handed subjects were available in OASIS. Left-handed subjects should be included in future studies to verify our hypothesis about AD-related asymmetric brainstem atrophy. Third, the modest sample size requires us to enroll more samples in the study to verify findings in the future even though 81 subjects were included from the ADNI dataset.

Conclusion

VBM is widely used in morphometric analysis of WM and GM due to its ability to determine focal differences in specific brain structure anatomy. We used VBM to analyze the brainstems of AD patients using a dedicated protocol, which can also be easily extended to other brain structures. Compared with NC, patients in the early stage of AD have atrophy of the bilateral pons and left part of the midbrain. The left part of the midbrain of the patients in the very mild AD group (CDR = 0.5) showed atrophy earlier in the brainstem. Structural atrophy in the midbrain and pons may be one site of early AD-related pathological changes.

Author contributions Author contributions included conception and study design (Wenpeng Gao and Xiaoguang Chen), data collection or acquisition (Xiaoxi Ji, Hong Zhang and Yingjie He), statistical analysis (Xiaoxi Ji, Hui Wang and Minwei Zhu), interpretation of results (Xiaoxi Ji, Hui Wang, Minwei Zhu, Wenpeng Gao), drafting the manuscript work or revising it critically for important intellectual content (Xiaoxi Ji, Minwei Zhu, Wenpeng Gao, Xiaoguang Chen and Yili Fu) and approval of final version to be published and agreement to be accountable for the integrity and accuracy of all aspects of the work (All authors).

Funding information This study was funded by the Science and Technology Cooperation Direction Project of Hainan Key Research and Development Plan (grant number ZDYD2019207) and National Natural Science Foundation of China (grant numbers 81171304, 81201150 and 81500924). It was also supported by Sanya Key Laboratory Construction (grant number L1232) and Natural Science Foundation of Hainan Province of China (grant number 20158306). The OASIS dataset used in this work was funded by grants (P50 AG05681, P01 AG03991, R01 AG021910, P50 MH071616, U24 RR021382, R01 MH56584). Data used in preparation of this article were obtained from the ADNI database (adni.loni.usc.edu). As such, the investigators within the ADNI contributed to the design and implementation of ADNI and/or provided data but did not participate in analysis or writing this report. A complete listing of ADNI investigators can be found at http://adni.loni.usc.edu/wp-content/uploads/how_to_apply/ADNI_Acknowledgement_List.pdf.

Compliance with ethical standards

This article does not contain any studies with human participants performed by any of the authors.

Conflict of interest The authors declare they have no conflict of interest.

References

- Ashburner, J., & Friston, K. J. (2000). Voxel-based morphometry—the methods. *Neuroimage*, *11*, 805–821.
- Attems, J., Thomas, A., & Jellinger, K. (2012). Correlations between cortical and subcortical tau pathology. *Neuropathology and Applied Neurobiology*, *38*, 582–590.
- Buckner, R. L., Head, D., Parker, J., Fotenos, A. F., Marcus, D., Morris, J. C., & Snyder, A. Z. (2004). A unified approach for morphometric and functional data analysis in young, old, and demented adults using automated atlas-based head size normalization: Reliability and validation against manual measurement of total intracranial volume. *Neuroimage*, *23*, 724–738.
- Busatto, G. F., Diniz, B. S., & Zanetti, M. V. (2008). Voxel-based morphometry in Alzheimer's disease. *Expert Review of Neurotherapeutics*, *8*, 1691–1702.
- Celle, S., Delon-Martin, C., Roche, F., Barthélémy, J. C., Pépin, J. L., & Dojat, M. (2016). Desperately seeking grey matter volume changes in sleep apnea: A methodological review of magnetic resonance brain voxel-based morphometry studies. *Sleep Medicine Reviews*, *25*, 112–120.
- Chetelat, G., & Baron, J. C. (2003). Early diagnosis of Alzheimer's disease: Contribution of structural neuroimaging. *NeuroImage*, *18*, 525–541.
- Fischl, B. (2012). Freesurfer. *Neuroimage*, *62*, 774–781.
- Fotenos, A. F., Snyder, A. Z., Girton, L. E., Morris, J. C., & Buckner, R. L. (2005). Normative estimates of cross-sectional and longitudinal brain volume decline in aging and AD. *Neurology*, *64*, 1032–1039.
- Grinberg, L., Rüb, U., Ferretti, R., Nitrini, R., Farfel, J., Polichiso, L., Gierga, K., Jacob-Filho, W., Heinsen, H., & Brazilian Brain Bank Study Group. (2009). The dorsal raphe nucleus shows phospho-tau neurofibrillary changes before the transentorhinal region in Alzheimer's disease. A precocious onset? *Neuropathology and Applied Neurobiology*, *35*, 406–416.
- Grinberg, L. T., Rueb, U., & Heinsen, H. (2011). Brainstem: Neglected locus in neurodegenerative diseases. *Frontiers in Neurology*, *2*, 42.
- Grudzien, A., Shaw, P., Weintraub, S., Bigio, E., Mash, D. C., & Mesulam, M. M. (2007). Locus coeruleus neurofibrillary degeneration in aging, mild cognitive impairment and early Alzheimer's disease. *Neurobiology of Aging*, *28*, 327–335.
- Hellström-Lindahl, E., Viitanen, M., & Marutle, A. (2009). Comparison of A β levels in the brain of familial and sporadic Alzheimer's disease. *Neurochemistry International*, *55*, 243–252.
- Hwang, J., Kim, J., Han, Y., & Park, H. (2011). An automatic cerebellum extraction method in T1-weighted brain MR images using an active contour model with a shape prior. *Magnetic Resonance Imaging*, *29*, 1014–1022.
- Karas, G., Scheltens, P., Rombouts, S., van Schijndel, R., Klein, M., Jones, B., van der Flier, W., & Barkhof, F. (2007). Precuneus atrophy in early-onset Alzheimer's disease: a morphometric structural MRI study. *Neuroradiology*, *49*, 967–976.
- Kinkingnehun, S., Sarazin, M., Lehericy, S., Guichart-Gomez, E., Hergueta, T., & Dubois, B. (2008). VBM anticipates the rate of progression of Alzheimer disease: A 3-year longitudinal study. *Neurology*, *70*, 2201–2211.
- Lee, J. H., Ryan, J., Andreescu, C., Aizenstein, H., & Lim, H. K. (2015). Brainstem morphological changes in Alzheimer's disease. *Neuroreport*, *26*, 411–415.
- Marcus, D. S., Wang, T. H., Parker, J., Csernansky, J. G., Morris, J. C., & Buckner, R. L. (2007). Open access series of imaging studies (OASIS): Cross-sectional MRI data in young, middle aged, nondemented, and demented older adults. *Journal of Cognitive Neuroscience*, *19*, 1498–1507.
- Morris JC (1993) The clinical dementia rating (CDR): Current version and scoring rules. *Neurology*, *43*, 2412b–2414b.
- Mrzilková, J., Zach, P., Bartoš, A., Tintěra, J., & Řípková, D. (2012). Volumetric analysis of the pons, cerebellum and hippocampi in patients with Alzheimer's disease. *Dementia and Geriatric Cognitive Disorders*, *34*, 224–234.
- Mungas, D., Reed, B. R., Jagust, W. J., DeCarli, C., Mack, W. J., Kramer, J. H., Weiner, M. W., Schuff, N., & Chui, H. C. (2002). Volumetric MRI predicts rate of cognitive decline related to AD and cerebrovascular disease. *Neurology*, *59*, 867–873.
- Musa, G., Henríquez, F., Muñoz-Neira, C., Delgado, C., Lillo, P., & Slachevsky, A. (2017). Utility of the neuropsychiatric inventory questionnaire (NPI-Q) in the assessment of a sample of patients with

- Alzheimer's disease in Chile. *Dement Neuropsychol*, 11(2), 129–136.
- Paul, A. Y., Joseph, P., Heather, C. H., Rachel, G. S., Sean, H., James, C. G., & Guido, G. (2006). User-guided 3D active contour segmentation of anatomical structures: Significantly improved efficiency and reliability. *Neuroimage*, 31, 1116–1128.
- Ridgway, G. R., Henley, S. M., Rohrer, J. D., Scahill, R. I., Warren, J. D., & Fox, N. C. (2008). Ten simple rules for reporting voxel-based morphometry studies. *NeuroImage*, 40, 1429–1435.
- Rodríguez, J. J., Noristani, H. N., & Verkhatsky, A. (2012). The serotonergic system in ageing and Alzheimer's disease. *Progress in Neurobiology*, 99, 15–41.
- Rüb, U., Del, T. K., Schultz, C., Thal, D., Braak, E., & Braak, H. (2000). The evolution of Alzheimer's disease-related cytoskeletal pathology in the human raphe nuclei. *Neuropathology and Applied Neurobiology*, 26, 553–567.
- Rubin, E. H., Storandt, M., Miller, J. P., Kinschler, D. A., Grant, E. A., Morris, J. C., & Berg, L. (1998). A prospective study of cognitive function and onset of dementia in cognitively healthy elders. *Archives of Neurology*, 55, 395–401.
- Samuraki, M., Matsunari, I., Chen, W. P., Yajima, K., Fujikawa, A., Takeda, N., Nishimura, S., Matsuda, H., & Yamada, M. (2007). Partial volume effect-corrected FDG-PET and grey matter volume loss in patients with mild Alzheimer's disease. *European Journal of Nuclear Medicine and Molecular Imaging*, 34, 1658–1669.
- Schuff, N., Woerner, N., Boreta, L., Kornfield, T., Shaw, L., Trojanowski, J., Thompson, P. M., Jack Jr., C. R., Weiner, M. W., & Alzheimer's Disease Neuroimaging Initiative. (2009). MRI of hippocampal volume loss in early Alzheimer's disease in relation to ApoE genotype and biomarkers. *Brain*, 132, 1067–1077.
- Shi, F., Liu, B., Zhou, Y., Yu, C., & Jiang, T. (2009). Hippocampal volume and asymmetry in mild cognitive impairment and Alzheimer's disease: Meta analyses of MRI studies. *Hippocampus*, 19, 1055–1064.
- Tae, W. S., Kim, S. S., Lee, K. U., Nam, E. C., & Kim, K. W. (2008). Validation of hippocampal volumes measured using a manual method and two automated methods (Freesurfer and IBASPM) in chronic major depressive disorder. *Neuroradiology*, 50, 569–581.
- Takao, H., Hayashi, N., & Ohtomo, K. (2014). Effects of study design in multi-scanner voxel-based morphometry studies. *NeuroImage*, 84, 133–140.
- Walhovd, K. B., Fjell, A. M., Reinvang, I., Lundervold, A., Dale, A. M., Eilertsen, D. E., Quinn, B. T., Salat, D., Makris, N., & Fischl, B. (2005). Effects of age on volumes of cortex, white matter and subcortical structures. *Neurobiology of Aging*, 26, 1261–1270.
- Wang, J. Y., Ngo, M. M., Hessel, D., Hagerman, R. J., & Rivera, S. M. (2016). Robust machine learning-based correction on automatic segmentation of the cerebellum and brainstem. *PLoS One*, 11, e0156123.
- Weier, K., Beck, A., Magon, S., Amann, M., Naegelin, Y., Penner, I. K., Thürling, M., Aurich, V., Derfuss, T., Radue, E. W., Stippich, C., Kappos, L., Timmann, D., & Sprenger, T. (2012). Evaluation of a new approach for semi-automatic segmentation of the cerebellum in patients with multiple sclerosis. *Journal of Neurology*, 259, 2673–2680.
- Wilson, R. S., Nag, S., Boyle, P. A., Hizek, L. P., Yu, L., Buchman, A. S., Shah, R. C., Schneider, J. A., Arnold, S. E., & Bennett, D. A. (2013). Brainstem aminergic nuclei and late-life depressive symptoms. *JAMA Psychiatry*, 70, 1320–1328.
- Wright, I. C., McGuire, P. K., Poline, J. B., Travere, J. M., Murray, R. M., Frith, C. D., Frackowiak, R. S., & Friston, K. J. (1995). A voxel-based method for the statistical analysis of gray and white matter density applied to schizophrenia. *Neuroimage*, 2, 244–252.
- Zhang, Y., Brady, M., & Smith, S. (2001). Segmentation of brain MR images through a hidden Markov random field model and the expectation maximization. *IEEE Trans. on Medical Imaging*, 20, 45–57.
- Zhu, M., Gao, W., Wang, X., Chen, S., & Lin, Z. (2012). Progression of corpus callosum atrophy in early stage of Alzheimer's disease: MRI based study. *Academic Radiology*, 19, 512–517.
- Zhu, M., Wang, X., Gao, W., Chen, S., Ge, H., Shen, H., & Lin, Z. (2014). Corpus callosum atrophy and cognitive decline in early Alzheimer's disease: Longitudinal MRI. *Dementia and Geriatric Cognitive Disorders*, 37, 214–222.